

The Creation of AGB Fallback Shells

Zhuo Chen^{1*}, Adam Frank^{1†}, Eric G. Blackman^{1,2‡} and Jason Nordhaus^{3,4§}

¹*Department of Physics and Astronomy, University of Rochester, Rochester NY, 14627*

²*School of Natural Sciences, Einstein Drive, Institute for Advanced Study, Princeton NJ, 08540*

³*National Technical Institute for the Deaf, Rochester Institute of Technology, 52 Lomb Memorial Drive, Rochester NY, 14623*

⁴*Center for Computational Relativity and Gravitation, Rochester Institute of Technology, One Lomb Memorial Drive, Rochester NY, 14623*

Written in 2015 April 30

ABSTRACT

The possibility that mass ejected during Asymptotic Giant Branch (AGB) stellar evolution phases falls back towards the star has been suggested in applications ranging from the formation of accretion disks to the powering of late-thermal pulses. In this paper, we seek to explicate the properties of fallback flow trajectories from mass-loss events. We focus on a transient phase of mass ejection with sub-escape speeds, followed by a phase of a typical AGB wind. We solve the problem using both hydrodynamic simulations and a simplified one-dimensional analytic model that matches the simulations. For a given set of initial wind characteristics, we find a critical shell velocity that distinguishes between "shell fallback" and "shell escape". We discuss the relevance of our results for both single and binary AGB stars. In particular, we discuss how our results help to frame further studies of fallback as a mechanism for forming the substantial population of observed post-AGB stars with dusty disks.

Key words: stars: AGB and post-AGB — stars: winds, outflows — methods: numerical

1 INTRODUCTION

The possibility that some material ejected during the AGB mass loss stage falls back onto the star has been the subject of a number of studies, motivated by both theoretical and observational considerations (Bujarrabal Alcolea & Neri 1998; Soker 2001; Van Winckel et al. 1998; Van Winckel 1999; Waters, Trams & Waelkens 1992; Zijlstra et al. 2001).

The discovery of a population of post-AGB stars hosting dusty, long-lived disks is a puzzle for standard stellar evolution theory as it is not clear how these disks originate (Clayton et al. 2014; Su et al. 2007; Venn, K. A. et al. 2014). Given that some occur in binaries, it has been assumed that most if not all, are the result of some form of mass transfer (Bujarrabal et al. 2005; Dermine et al. 2012; Hinkle et al. 2007; Malek & Cami 2014; Van Winckel et al. 2009).

Theoretically, there is diverse interest in AGB mass-loss fallback. Asking when the return of matter can significantly influence post-AGB evolution, Soker (2001) considered the forces acting on back-flowing material in order to set limits on when such fallback can occur (though no trajectories were calculated). In order for back flow to play a role

in post-AGB and Planetary Nebulae (PN) evolution, that study concluded that the fallback mass should be high, the ejected velocity should be low, and that the mass should be concentrated along the AGB equator.

For a spherically symmetric case, thermal pulses or fuel limited relaxation oscillations may be a source of such mass loss (Van Horn et al. 2003). In Frankowski & Soker (2009), backflows were invoked as a means of creating very late thermal pulses (VLTP). Hajduk et al. (2007) also considered the possibility that mass accretion can induce a VLTP in the context of the old nova CK Vul where the mass is assumed to come from a companion. Frankowski & Soker (2009), however, considered the accreted mass falling back from AGB wind material that had become part of a planetary nebula.

In Soker (2008), the possibility for fallback to occur via a stellar "evanescent zone" was explored where, in addition to the escaping wind, gas parcels do not reach the escape velocity but rise slowly through the zone and then fall back. Wind and bound gas were found to exist simultaneously out to distances of ~ 100 AU.

Backflow has also been proposed as a mechanism for slowing evolution along post-AGB evolutionary tracks (Zijlstra et al. 2001) and for depleting post-AGB dust stars of refractory elements (e.g. Van Winckel et al. (1998)).

Explaining the observations of disks around post-AGB stars (discussed above) has, however, been one of the main

* E-mail: zchen25@ur.rochester.edu

† E-mail: a frank@pas.rochester.edu

‡ E-mail: blackman@pas.rochester.edu

§ E-mail: nordhaus@astro.rit.edu

reasons for exploring studies of fallback during AGB mass loss. Such a suggestion was part of the motivation driving the Soker (2001) paper. In addition, Akashi & Soker (2007) suggested that circumbinary rotating disks can also be formed from slow-AGB-wind material that is pushed back towards the star by wide jets emanating from one of the stars (i.e. collimated PPN or PN outflows Bujarrabal Alcolea & Neri (1998)).

A natural means for generating fallback in the context of binary stars however may be common envelope (CE) evolution. Both simulations and analytic models indicate that some fraction of the material expelled from the envelope may not escape the binary system (Nordhaus & Blackman 2006; Nordhaus et al. 2007; Kashi & Soker 2011; Ricker & Tamm 2012; Passy et al. 2012). Some of this material is, therefore, expected to fall back after the CE mass ejection event. This can occur even when the CE event involves a low-mass object such as a massive planet being swallowed by an AGB star (Nordhaus & Blackman 2006). Planetary companions to main-sequence stars are plentiful and those orbiting within ~ 10 AU can be expected to plunge into their host stars during the giant branches (Nordhaus et al. 2010, 2011; Nordhaus & Spiegel 2013). In such cases, material would be ejected over short timescales (a shell) with sub-escape velocities ($V_s < V_{esc}$). Thus, it is possible that circumbinary disks are the result of CE ejections in which some fraction of the envelope is ejected at sub-escape speeds which may drop back to be shaped into a disk.

Given the interest in fallback on the AGB, in this paper we attempt to gain some insight into the dynamics of fallback shells by considering only the radial trajectories of the expelled gas. Of particular interest is the response of a sub-escape velocity shell to internal driving by the AGB wind which would likely follow the shell ejection. Note that we do not explicitly specify or model the origin of the mass-loss history as our goal here is simply to study the dynamics of the shell after its initial ejection from the star. In Sect. 2, we introduce our hydrodynamic model and methods to solve the problem. In Sect. 3.1, we present the results of full hydrodynamic simulations. In Sect. 3.2 we present a semi-analytic model and compare it with the simulation results as well as present a zeroth order estimate of the critical velocity of the shell that distinguish collapse or escape trajectories.

2 METHOD AND MODEL

We use the ASTROBEAR adaptive mesh refinement (AMR) code to solve the hydrodynamic equations (Cunningham et al. 2009; Carroll-Nellenback et al. 2013). AMR is a computational technique that divides a computational cell into $2^{dimension}$ child cells when the physical condition suggests to (usually high gradient).

$$\frac{\partial \rho}{\partial t} + \nabla \cdot (\rho \mathbf{v}) = 0 \quad (1)$$

$$\frac{\partial \rho \mathbf{v}}{\partial t} + \nabla \cdot (\rho \mathbf{v} \mathbf{v}) = -\nabla P - \frac{GM\rho}{r^2} \hat{\mathbf{r}} \quad (2)$$

$$P = nk_b T \quad (3)$$

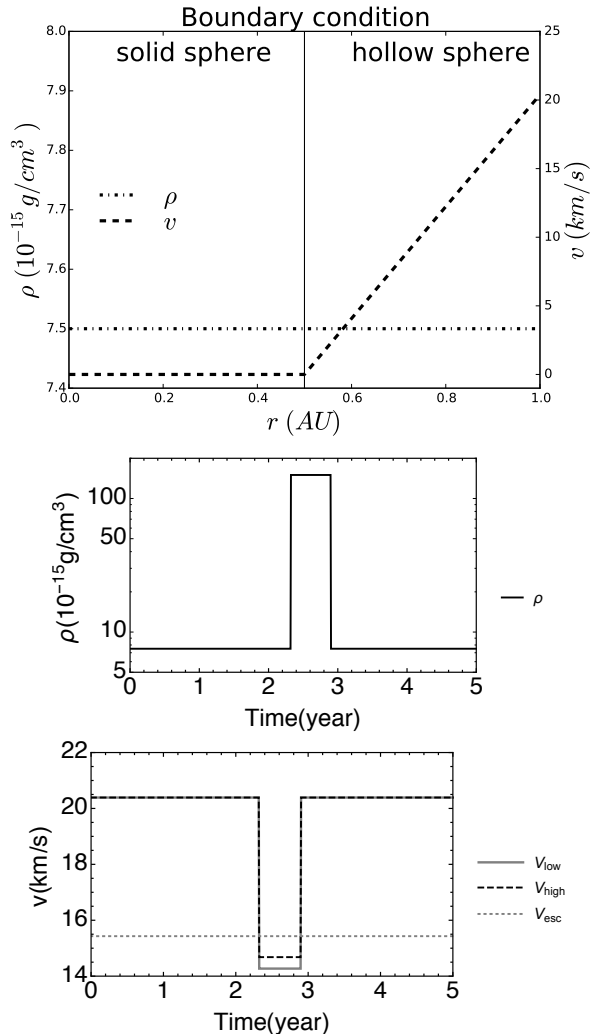


Figure 1. First panel shows the boundary condition of the star when it emits stellar wind. Second and third panels show time dependence of density and velocity.

where $n = \rho/m_{mean}$ is the particle number density and $m_{mean} = 1.3 m_H$ is the mean particle mass.

We begin with an AGB star at the origin and allow it fill the grid with a pre-shell wind. The mass of the star is $1 M_\odot$. The escape velocity at 1 AU from the center of the star is $v_{esc} = 15.43$ km/s. We account for radiation pressure within the gas and dust by using an the effective stellar gravity of $\alpha GM_\odot/r^2$ with $\alpha = 0.134$. However, we do not specify the dust species and evolution in the simulation, that is, we only assume a steady state distribution of dust. The whole region can be optically thin which will be examined.

$$f_{rad} = \frac{\rho(r)\kappa_{total}S(r)}{c} = \frac{(1-\alpha)GM_\odot\rho(r)}{r^2} \quad (4)$$

therefore,

$$\tau = \int_{1AU}^{30AU} \rho(r)\kappa_{total}dr = \int_{1AU}^{30AU} \frac{4\pi(1-\alpha)GM\rho(r)c}{L} dr \quad (5)$$

where $\rho(r)$ is the density of wind at radius of r , κ_{total} is the total mass weighted opacity, $S(r)$ is the radiation intensity, L is the bolometric luminosity of the AGB star and τ is the

optical depth. In our simulation, the pre-shell wind is driven into the grid at $r_0 = 1 \text{ AU}$ with velocity $v_0 = 20.39 \text{ km/s}$. The wind has an injection density of $\rho_0 = 7.5 \times 10^{-15} \text{ g/cm}^3$ yielding a mass loss rate of $\dot{M}_0 = 6.84 \times 10^{-7} M_\odot \text{ yr}^{-1}$. By mass conservation law,

$$\rho_0 v_0 (AU)^2 = \rho(r) v(r) r^2 \quad (6)$$

we can substitute equation (6) into equation (5) and for computational convenience, eliminate v_0 and $v(r)$ on both side since they are on the same order of magnitude. For a typical $L = 1500 L_\odot$ AGB star, we can get that $\tau < 1$. Obviously, if we lower all the wind density (as well as the mass loss rate) by a factor of several, the whole region would be optically thin and the hydrodynamic property would not change since equations (1,2,3) all scale linearly with the density.

The simulation is isothermal and the temperature is 100 K . This yields an initial Mach number of $Mach = 22.4$. The boundary of the star is a sphere and the inner condition do not change upon the variation of outer condition. We divide the inner region of the star into two parts, a solid sphere and a spherically concentric shell (Shown in the first panel in Figure1.). The solid sphere has time dependent but uniform density and zero velocity while the concentric shell has the same time dependent uniform density but linearly increasing velocity from the inner side to the outer side. The inner side velocity is zero and the outer side velocity is the wind velocity. R and z axes are both reflective boundaries while top and right edge of the computational box only allow outflow, so any negative velocity at the boundary is set to be zero. The free fall time at the boundary is 80 yrs and the sound speed is 0.90 km/s . Given that the initial ambient density is extremely low and that constant wind will fill the grid before the dense shell outflow, the boundary condition will have tiny effect on the simulation.

After the wind fills the grid we drive a dense shell from the star. The shell episode lasts from $t_1 = 2.32 \text{ yr}$ to $t_2 = 2.90 \text{ yr}$. During the episode, the density rises to $1.5 \times 10^{-13} \text{ g/cm}^3$. The velocity drops to either $v_{low} = 14.27 \text{ km/s}$ or $v_{high} = 14.68 \text{ km/s}$ for the two cases we present here. As we will see, these two cases bracket a bifurcation in the evolution of the ejected shell. Both of these cases have $v_s < v_{esc}$ and in both cases approximately $M = 5.6 \times 10^{-6} M_\odot$ is ejected in the shell. For computational convenience, we approximate the time dependence of density and velocity during shell ejections as step functions.

After the shell ejection terminates, we resume the steady wind (which we subsequently refer to as a "post-shell wind"). The second and the third panels in Figure1 show the density and velocity history for our simulations. The figures show that in both simulations, the velocity during the shell ejection is sub-escape at the stellar boundary where mass flows into the grid.

Because ASTROBEAR does not have 1-D capacities, we run our code in (r, z) cylindrical symmetry (2.5D) covering one quarter of the total plane and average over the spherical angle θ . Thus we impose reflecting boundaries at $r = 0$ and $z = 0$. The top and right boundaries use outflow boundary conditions allowing material to leave the grid. The winds and shell are injected into the grid via a spherical "surface" boundary condition at r_0 . The computational domain is $24 \times 24 \text{ AU}^2$ and consists of a 240×240 base grids plus 4 levels

of AMR. Thus the "effective" resolution of our simulations is $(3840)^2$.

3 RESULTS

3.1 Simulations from AstroBEAR

In what follows we present two examples from a larger suite of simulations chosen to bracket the transition from escape to fall-back modes of the ejected shell. In Figure 2 and 3, we present 1D profiles of density and velocity at four different times in the evolution of the simulations. We take the profiles along the 45-degree line in the $r - z$ plane. We also plot the local escape velocity for reference.

The four panels in Figure2 show frames from the simulation with the lower shell ejection velocity $v_{shell} = 14.27 \text{ km/s}$ (note with time increases from top to bottom). The simulation begins with the steady wind filling the grid then the pulse of high density, sub-escape material (the shell) is launched at 2.32 yr . In panel (a) we see the density and velocity profiles at $t = 5.23 \text{ yr}$. Note that the steep rise in velocity between the origin and $r = 1 \text{ AU}$ represents the inflow boundary where the stellar flow is injected into the grid. In this region we also see that the density is held constant.

In the first panel between 1 AU and 4 AU , the density of the steady wind ejected after the mass loss "pulse" drops continuously due to the geometric expansion of the gas. The velocity also falls due to deceleration by the gravity of the AGB star. Thus since $\rho \propto \dot{M}_w / v_w(r) r^2$, the wind density in this region falls off more slowly than $\rho(r) \propto r^{-2}$.

At $r = 4 \text{ AU}$, the steady post-pulse wind encounters the inner edge of the shell ejected during the brief pulse high mass loss. From this shock interface to approximately $r = 6 \text{ AU}$ we see shell material. Note that the velocity in this region is below the local escape velocity of the AGB star. Between $r = 6 \text{ AU}$ and $r = 9 \text{ AU}$ we see a steady drop in the density and steady increase in the velocity. This region represents a rarefaction wave running from the denser but slower moving shell material and the supersonic, supra-escape pre-shell wind ejected before the pulse. The most important point to note in panel (a) of figure 2 is the presence of the shock at $r = 4 \text{ AU}$. This shock wave represents a transfer of momentum from the post-pulse wind into the shell which causes varying degrees of shell acceleration depending, on the relative momenta of the wind and shell.

At $t = 11.04 \text{ yr}$, we see the dense shell is has expanded outward. The shock bounding the shell and the post-shell wind is now at $r = 6 \text{ AU}$. The boundary between the shell and pre-shell wind has expanded off the grid. Note however that the velocity of the shell is just above $v = 0$. Thus the shell has been almost entirely decelerated and is reaching its maximum radial excursion.

By $t = 16.86 \text{ yr}$, the velocity of the shell has fallen below $v = 0$. At this point the shell has begun to fall back towards the star. By $t = 22.09 \text{ yr}$, the shock boundary between the wind and the shell is at $r = 3 \text{ AU}$ as the shell continues to collapse back towards the star. Note that for all positions above this radius we see $v < 0$ which implies all material at these larger radii is moving radially inward as well. This makes sense because of the rarefaction between

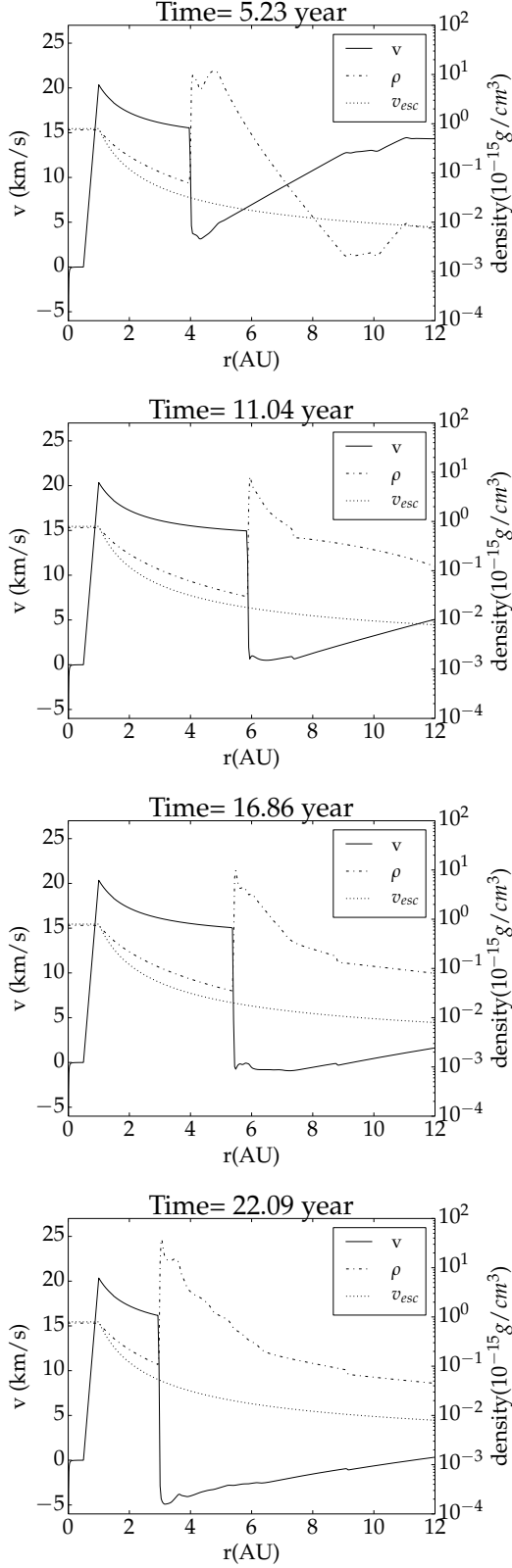


Figure 2. Time evolution of shell with initial shell velocity $v_{low} = 14.27 \text{ km/s}$. The shell finally falls back.

the shell material and the pre-pulse wind. Since the right and top boundary is made to only allow outflow, it must be different from a self-consistent boundary. However, our simulation zone is large enough to keep the region we are interested unaffected. If the gas flows in from the boundary right after the velocity become zero, an error - induced by the artificial boundary condition - will travel at the sound speed which is 0.90 km/s . However, the error does not have enough time to travel from the boundary (24 AU) to 12 AU in just 22 yrs . So the fluid motion in $12 \times 12 \text{ AU}^2$ is not adversely affected by the boundary.

Finally, note that the sound speed becomes greater than shell speed as it decelerates ($cs > v$). During this period we have a subsonic flow ($Mach < 1$) where pressure force become important and we see an expansion of the shell width with very slow bulk radial motion.

In Figure 3, we show radial profiles of density and velocity for the simulation with a higher initial shell velocity. In the first panel, taken at $t = 10.46 \text{ yr}$, the shock boundary between post-shell wind and the shell is located at about $r = 7.5 \text{ AU}$. Note the velocity of the shell is below the local escape velocity. As the post-shell wind continues to impart momentum to the shell, we observe a different evolution. In subsequent frames, the shell does not stall but is slowly driven outward. By $t = 31.39 \text{ yr}$, the shell has reached $r = 16 \text{ AU}$ and its velocity is now just below the local escape value. By $t = 41.85 \text{ yr}$ the shell has been almost entirely pushed off the grid and has achieved a speed in excess of the local escape velocity. Thus we find a shell ejected with $v_{shell} = 14.27 \text{ km/s}$, will fall back onto the star. The shell with $v_{shell} = 14.68 \text{ km/s}$, which is also below the escape velocity, at the launch radius, will escapes.

3.2 A One Dimensional Spherical Model

In order to understand the transition between models with shells that escape under the action of the post-shell wind and those which fall back onto the star, we now derive a simplified analytical treatment of the problem.

To compare our $2.5D$ simulation with a $1D$ analytic model, we use fluid tracers in the simulations to track shell material. We use tracer mass weighted averages of the tracer's radial extent as a measure of shell's position vs time $r_s(t)$.

$$r_s = \frac{\int_{1AU}^{30AU} \rho_{tracer} r^3 dr}{\int_{1AU}^{30AU} \rho_{tracer} r^2 dr} \quad (7)$$

We assume that the initial velocity and density of the shell are v_s and ρ_s respectively. For the shell initial mass we have:

$$m_s = 4\pi r^2 \rho_s v_s \Delta t, \quad (8)$$

where Δt is the time interval of injection. The post-shell wind has initial velocity v_0 and initial density ρ_0 at the launch point. For a steady spherical wind, mass conservation implies:

$$4\pi r^2 \rho_w v_w = 4\pi r_0^2 \rho_0 v_0 \quad (9)$$

Thus the wind density will fall off as: $\rho_w = (r_0^2 \rho_0 v_0) / (r^2 v_w)$.

We calculate the evolution of the shell velocity v_s from the momentum equation (2). We assume that pressure forces are negligible with $\| -\nabla P \| \ll \| \frac{GM\rho}{r^2} \|$. This assumption

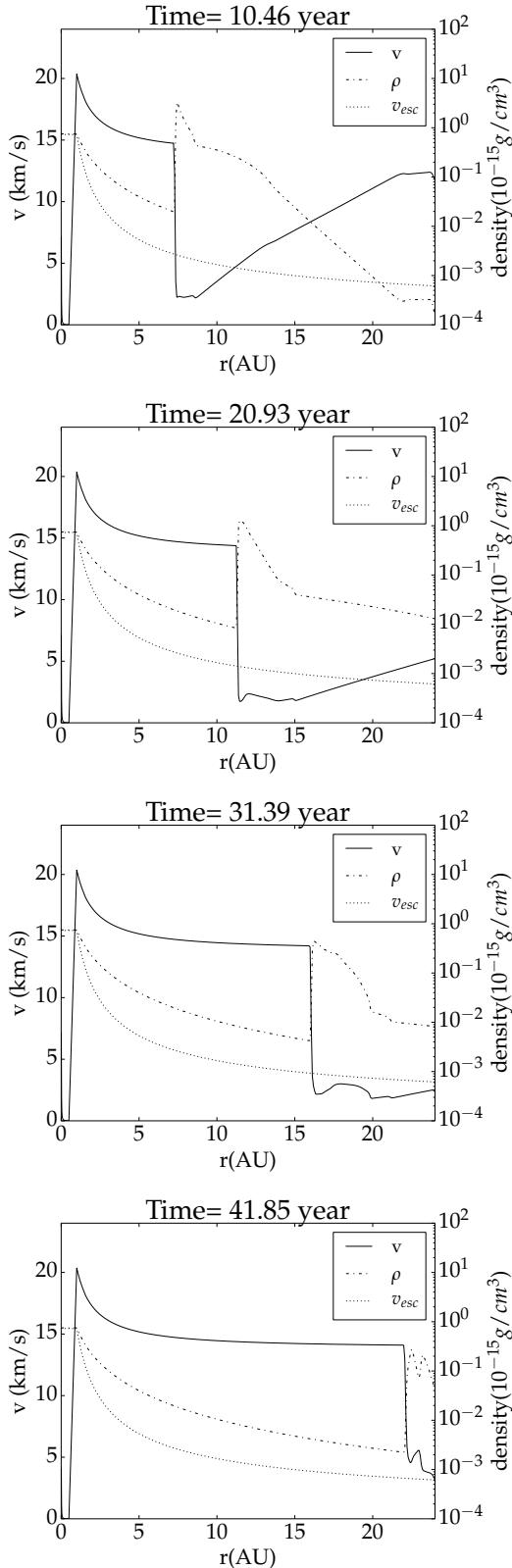


Figure 3. Time evolution of shell with initial shell velocity $v_{high} = 14.68 \text{ km/s}$. The shell exceeds the escape velocity

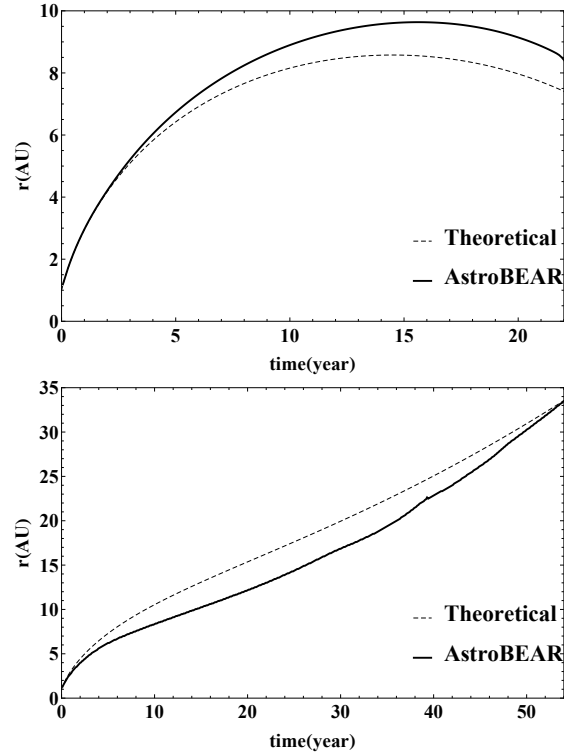


Figure 4. Results of trajectories of the shell from ASTROBEAR and analytic model. Pulsation velocities are $v_{low} = 14.27 \text{ km/s}$ and $v_{high} = 14.68 \text{ km/s}$ respectively.

is valid at all times except during the brief stalling of the shell that initiates fallback. The momentum equation thus becomes

$$\frac{\partial \rho \mathbf{v}}{\partial t} + \nabla \cdot (\rho \mathbf{v} \mathbf{v}) = -\frac{GM\rho}{r^2} \hat{\mathbf{r}}. \quad (10)$$

We must track the velocity of the wind gas before it impacts the dense shell as it is subject to deceleration due to gravity,

$$v_w(r) = \sqrt{\mathbf{v}_0^2 - \frac{2GM}{r_0} - \frac{2GM}{r}} \quad (11)$$

For the momentum of the shell we write a discrete form of the momentum equation as

$$m_s(t+dt) \mathbf{v}_s(t+dt) = m_s(t) \mathbf{v}_s(t) + dm_w \mathbf{v}_w - \frac{GMm_s}{r^2} \hat{\mathbf{r}} dt \quad (12)$$

where the second term on the right represents momentum added to the shell by the wind in a time dt and the third term represents deceleration due to gravity. More specifically, for the wind mass added to the shell we have,

$$dm_w = 4\pi r^2 \rho (v_w(t) - v_s(t)) dt \quad (13)$$

so that

$$m_s(t+dt) = m_s(t) + dm_w \quad (14)$$

Using the evolution of the shell velocity:

$$\mathbf{v}_s(t+dt) = \frac{m_s(t) \mathbf{v}_s + dm_w \mathbf{v}_w - \frac{GMm_s}{r^2} \hat{\mathbf{r}} dt}{m_s(t+dt)} \quad (15)$$

Using Eqs. (9) and (10), we divide equation (8) by $m_s(t+dt)$ and solve it numerically to find the trajectory

of the shell $r(t)$ for any set of initial conditions. In particular we look for the critical value of the initial shell velocity v_c that distinguishes between fall back and escape. Evaluation of equation (15) shows that for the inputs used in the simulations, the critical initial shell velocity is $v_c = 14.50 \text{ km/s}$. Figure 4 shows a comparison of the $r_s(t)$ for the analytic model and for simulations (i.e. $v_0 < v_c$ and $v_0 > v_c$). The analytic model does quite a good job of recovering the behavior seen in the simulations in both cases.

We can also estimate v_c even more simply by first approximating the turning point of the shell in the fall back case. Here assume that the mass of the shell is constant and neglect the effect of post-shell wind. This gives us a ballistic approximation for the maximum radius of the shell r_m . We then assume that the ram pressure of the steady wind must be large enough to support the shell against gravity at this radius if the wind is to stop the shell from falling back. This yields

$$\frac{Gm_s M}{r^2} = \frac{dp_{ram}}{dt} \quad (16)$$

where p_{ram} is the the magnitude of the ram momentum of the wind given by

$$p_{ram} = 4\pi\rho r_m^2 v_w^2 = 4\pi\rho_0 r_0^2 v_0 v_w = \dot{M} v_w \quad (17)$$

Note that v_w is a function of r from Eq. (11). Note also that r_m is determined by v_0 according to our assumption of ballistic motion, namely it corresponds to the radius where the velocity vanishes. Then force balance gives

$$r_m = \frac{-2r_0 GM}{v_0^2 r_0 - 2GM}, \quad (18)$$

$$v_w = \sqrt{v_c^2 - \frac{2GM}{r_0} + \frac{2GM}{r_m}}, \quad (19)$$

Then using Eqs. (18), (19) and 8 in the form

$$m_s = 4\pi r_0^2 \rho_0 v_c \Delta t \quad (20)$$

in Eq. (16), we find v_c . The result is $v_c = 14.77 \text{ km/s}$ which is only 1.9% higher than the numerical result 14.50 km/s

4 SUMMARY AND DISCUSSION

We have presented a simple model for the evolution of a shell ejected with sub-escape velocity during a brief pulse of enhanced mass loss in an AGB star. The fate of the ejected shell depends on the acceleration to escape velocity via the action of the continuing steady AGB wind that follows the launching of the shell. Our 2.5D isothermal hydrodynamic simulations are compared with a spherically-symmetric analytic model for the time evolution of the shell. Both the analytic model and simulations closely support in their predictions for the value of the critical shell velocity v_c that delineates the bifurcation between escape and fall-back modes of shell evolution. Though in the presence of spherically symmetric radial temperature gradient, the diffusion rate will be different but the qualitative result that we find—a bifurcation of fall back vs. escape modes would still be expected.

Our results lay out the basic dynamics of fall-back shells and are relevant to any mechanism which ejects material with less than the local escape velocity. Our study also establishes the first step along the path to study post-AGB

disk formation via fall-back shells. Since AGB stars are slow rotators, we would expect that an ejected shell would not have enough angular momentum to establish a Keplerian disk at large radii. Thus ejected gas will either fall back onto the star or escape for isolated stars. In the case of a binary however, the material falling back onto the AGB star might gain enough angular momentum through gravitational interaction to form a Keplerian disk at large radii. This is a topic for future study.

ACKNOWLEDGMENTS

Financial support for this project was provided by the LLE at the University of Rochester, Space Telescope Science Institute grants HST-AR-11251.01-A, HST-AR-12128.01-A, HST-AR-12146.04-A; by the National Science Foundation under awards AST-0807363 and AST-1102738; by the Department of Energy under award de-sc0001063. EB acknowledges support from the Simons Foundation, and the IBM-Einstein fellowship fund at IAS. The CIRC at the University of Rochester provided computational resources. A special thanks to Baowei Liu and Jonathan Carroll-Nellenback.

REFERENCES

- Akashi M., Soker N., Behar E., Blondin J., 2007, MNRAS, 375, 137
 Bujarrabal V., Alcolea J., Neri R., 1998, ApJ, 504, 915
 Bujarrabal V., Castro-Carrizo A., & Alcolea J. et al., 2005, A&A, 441, 1031
 Clayton G. C., De Marco O., & Nordhaus J. et al., 2014, AJ, 147, 142
 Carroll-Nellenback J. J., Shroyer B., Frank A., Ding C., 2013, JCoPh, 236, 461
 Cunningham A. J., Frank A., & Varnière P. et al., 2009, ApJS, 182, 519
 Dermine T., Izzard, R. G., Jorissen A., & Van Winckel H., 2013, A&A, 551, A50
 Frankowski, A., & Soker, N. 2009, New Astron., 14, 654
 Hajduk M. et al., 2007, MNRAS, 378, 1298
 Hinkle K. H., Brittain S. D., & Lambert D. L., 2007, ApJ, 664, 501
 Kashi A., & Soker N., 2011, MNRAS, 417, 1466
 Malek S. E., & Cami J., 2014, AJ, 794, 113
 Nordhaus J., & Blackman E. G., 2006, MNRAS, 370, 2004
 Nordhaus J., Blackman E. G., Frank A., 2007, MNRAS, 376, 599
 Nordhaus, J., Spiegel, D. S., Ibgui, L., Goodman, J., & Burrows, A. 2010, MNRAS, 408, 631
 Nordhaus, J., Wellons, S., Spiegel, D. S., Metzger, B. D., & Blackman, E. G. 2011, Proceedings of the National Academy of Science, 108, 3135
 Nordhaus, J., & Spiegel, D. S. 2013, MNRAS, 432, 500
 Passy J. C., De Marco O. & Fryer C. L. et al., 2012, ApJ, 744, 52
 Ricker P. M., & Tamm R. E., 2012, ApJ, 746, 74
 Soker N., 2001, MNRAS, 382, 1081
 Soker N., 2008, arXiv:0801.3089
 Su K. Y. L., Chu Y.-H., & Rieke G. H. et al., 2007, ApJL, 657, 41

- Van Horn H. M., Thomas J. H., Frank A., Blackman E. G.,
2003, ApJ, 585, 983
- Van Winckel H., Waelkens C., Waters L. B. F. M., Molster
F. J., Udry S., Bakker E. J., 1998, A&A, 336, L17
- Van Winckel H., 1999, in Le Bertre T., Lebre A., Waelkens
C., eds, Proc. IAU Symp. 191, Asymptotic Giant Branch
Stars. Astron. Soc. Pac., San Francisco, p. 465
- Van Winckel H., Lloyd Evans T., & Briquet M. et al., 2009,
A&A, 505, 1221
- Venn K. A., Puzia T. H., & Divell M., 2014, ApJ, 791, 98
- Waters L. B. F. M., Trams N. R., Waelkens C., 1992, A&A,
262, L37
- Zijlstra A. A., Chapman J. M., te Lintel Hekkert P., Likkell
L., Comeron F., Norris R. P., Molster F. J., Cohen R. J.,
2001, MNRAS, 322, 280

This paper has been typeset from a $\text{T}_{\text{E}}\text{X}/\text{L}^{\text{A}}\text{T}_{\text{E}}\text{X}$ file prepared
by the author.